ELSEVIER

International Journal of Mass Spectrometry 185/186/187 (1999) 603–615

International Journal of Mass Spectrometry

Transition-metal C_{60} bonding by guided ion beam scattering

Yousef J. Basir, Scott L. Anderson*

Department of Chemistry, University of Utah, Salt Lake City, UT 84112, USA

Received 23 June 1998; accepted 28 July 1998

Abstract

Ion beam scattering techniques are used to examine interactions of transition-metal ions with C_{60} over the collision energy range from 1–100 eV. The metals studied are iron, manganese, chromium, molybdenum, and tungsten. For each metal ion, in addition to charge transfer and dissociative charge transfer, two distinct types of MC_{60}^+ complexes are observed. One forms with no activation barrier at low collision energies, is weakly bound (1–3 eV), and always decomposes by loss of metal. We attribute this to an exohedral coordination complex, as has been proposed by others who have seen this type of complex. A second type of MC_{60}^+ complex is observed at collision energies above ~10 eV. This high energy complex has a substantial activation barrier to formation, is chemically bound, and decomposes by loss of metal dicarbide (MC_2) or metal. We propose that this complex is a network bound structure, with the metal atom probably sitting above the fullerene surface, chemically bound to two or more carbon atoms. (Int J Mass Spectrom 185/186/187 (1999) 603–615) © 1999 Elsevier Science B.V.

Keywords: Fullerene; C_{60}; Transition-metal ions; Scattering

1. Introduction

Metal-fullerene interactions are of interest from the viewpoint of materials, inorganic chemistry, and because they apparently mediate/catalyze growth of carbon nanotubes. Chemically stable metallofullerenes have been prepared and studied by a variety of methods [1–6], including mass spectrometry [7–9], and electron paramagnetic resonance (EPR) spectroscopy [2,6,7,10]. Some metallo-fullerenes have been isolated in sufficient quantities [9,11–16] to allow characterization by methods such as x-ray diffraction [17], EXAFS [16,18,19], UV/VIS/IR spectroscopy [14], electron spin resonance (ESR) [4], and neutron activation [20].

There are three distinct binding arrangements for the interaction of heteroatoms with fullerenes. For most of the metallo-fullerenes studied, the binding is endohedral, i.e. the metal atom is trapped inside the carbon cage. It has been shown by Laskin et al. [21] that an endohedral neon atom has a minor effect on the cage binding, although lanthanum has a relatively stronger effect. Of interest for comparison with our results is the study by Pradeep et al. [16], who prepared bound FeC_{60} by carbon vaporization in an atmosphere containing $Fe(CO)_5$. His results with liquid chromatography/mass spectrometry (LC/MS), Mössbauer, and EXAFS suggest that an endohedrally bound species was formed with a near-zero oxidation state iron atom bound to the interior surface of the cage.

* Corresponding author.

Dedicated to Professor Michael T. Bowers on the occasion of his 60th birthday.

PII S1387-3806(98)14117-9

Metals can also bind to the outside of the fullerene cage, essentially as coordination complexes. Numerous transition metal complexes of fullerenes in aqueous solutions have been investigated, some of these metals having been Fe, Mo, Rh, and Ta [22], Ni, Pd, and Pt [23] and other transition metals [12]. In these complexes, the fullerenes act like polyalkenes and the metal atom is attached in a dihapto fashion to a 6–6 double bond of the fullerene [23,24]. These externally coordinated complexes have also been prepared in the gas phase by thermal or low energy ion molecule reaction [25–29]. It has been shown by Bohme and co-workers [27] that the mode of bonding between the metal and fullerene in these complexes is the same as the solution complexes.

Heteroatoms can also chemically bind to, or substitute for, carbon atoms in the fullerene network. Smalley and co-workers [1] were able to produce $C_{59}B$ by laser vaporization, where the boron atom was believed to be substituted for a carbon atom in the network. $C_{59}N^+$ has been observed in our lab following high energy impact of N^+ on C_{60}, and this was proposed to be a substitution compound as well [30]. Jarrold and co-workers [31,32] observed features that were interpreted as network-bound metal-fullerene ($n < 60$) complexes in mobility measurements. Since metal atoms are significantly larger than carbon, these species are believed to have the metal bound on the outside of the fullerene framework.

We have previously used ion beam scattering to probe fullerene interactions with rare gases [33–35], alkali cations [36,37], main group atoms, and small molecules [28,30,38,39]. This approach has allowed examination of charge transfer, dissociative charge transfer, endohedral penetration, trapping and escape, and chemical bond formation. In this article we report our results for the transition metal cations, Fe^+, Mn^+, Cr^+, Mo^+, and W^+ reacting with C_{60}. Note that we previously made preliminary reports of some of these experiments [28,29], but in this article we have more accurately defined the energy scale, and more carefully analyzed the binding energetics.

In our experiments, internally excited fullerene product species are produced, and these decay/cool by a variety of competing mechanisms. We are only directly sensitive to processes where the mass changes, including fragmentation by C_n loss ("evaporative cooling" [34,35,40–43], or loss of metal-containing fragments. The product branching observed in our experiments is determined by the competition between these fragmentation channels and other cooling mechanisms including radiation [44,45] and electron emission [37,46]. Because we are concerned with cooling of nascent C_{60}^{+*} and MC_{60}^{+*} cations, cooling by thermal electron emission is not a significant cooling mechanism, however, radiation is probably important.

For IR fluorescence Lifshitz and co-workers [47] assumed a radiative decay rate $k_r = 100$ photons/s with an average frequency of 1000 cm^{-1}. In our experimental time scale (few hundred μs) this is a negligible cooling channel. On the other hand, Kolodoney et al. [45] found that blackbody radiation was an effective cooling channel in their experiment, based on analysis of time-of-flight distributions of effusive molecular beams. For hot C_{60} with an initial temperature around 1990 K, a temperature decrease of 136 K was estimated in the 3 millisecond experimental time window. Similar results were observed by Campbell and co-workers who found that C_{60} molecules in their beam cool by both evaporative and radiative channels [48]. Consistent with Kolodney, Campbell and co-workers concluded that radiative cooling can influence the unimolecular reaction rates of fullerene ions in their experiment [49]. Andersen and co-workers [44] studied the radiative cooling of negatively charged fullerene ions by following the thermionic emission as a function of time after injection into the heavy-ion storage ring ASTRID. For C_{60}^- at ~1500 K they obtained a radiative cooling rate of ~190 eV/s, which is 2 orders of magnitude more than expected from infrared radiation. This is in rough agreement with the radiation intensity for neutral C_{60} at 1800 K estimated by Kolodney et al. and indicates that the additional electron in C_{60}^- probably does not play a decisive role in the radiative cooling.

For the present metal C_{60} systems, we do not have enough thermochemical information to analyze our experimental results to obtain quantitative M–C_{60}^+ binding energies. We will present a semiquantitative analysis in which we will neglect radiative cooling.

This allows our results to be compared directly with earlier studies of C_{60} decomposition that also neglected radiative cooling.

2. Experiment

The experimental arrangement and operating conditions have been described in detail elsewhere [50] and will only be summarized here. Fe^+, Mn^+, Cr^+, Mo^+, and W^+ were produced by electron bombardment ionization of the metal carbonyls $Fe(CO)_5$, $Mn_2(CO)_6$, $Cr(CO)_6$, $Mo(CO)_6$, and $W(CO)_6$ (Alfa). The carbonyl was degassed repeatedly, then the vapor was introduced into the ion source via a stainless capillary tube with flow rate controlled by a leak valve. To reduce decomposition of the carbonyl vapor in the inlet system, which gets heated by the ion source filament, the inlet tube is water cooled.

Electron ionization (60 eV) of organometallics can produce significant populations of ion excited states, and there are many excited states of transition metal ions, some of which are metastable [51–55]. The population of excited states depends on the transition metal used. It has been reported that only small fractions of Fe^+ metastable states (~3% with 0.5 eV above ground states) are formed in electron ionization (EI) of $Fe(CO)_5$ [54]. At the same time approximately 26% metastable excited states of Cr^+ ions were produced by 70 eV electron impact on $Cr(CO)_5$ [54]. Electron impact on $Mn_2(CO)_6$ produced 22% metastable excited states of Mn^+ ions [52]. Our experiments with electron impact energies less than 60 eV certainly allow production of excited states. Our source pressures and residence times are such that most nascent ions make several collisions with the carbonyl vapor, and this should deplete the excited state populations to some extent. No attempt was made to study the effect of these excited states on the reactions, however, the reactivity of the transition metal ions is quite high, and it is unlikely that even 10% excited state contamination would give an observable signature.

The mixture of ions generated in the source is injected into a radio-frequency octapole ion guide, then mass filtered by passage through a 90° magnetic sector. The reactant ion beam current after the magnetic sector is about one nano-ampere. The selected metal ion beam is then injected into a second octapole ion guide system that sets the collision energy. This ion guide serves both to guide the reactant ion beam through an oven containing the C_{60} vapor, and to collect both the reactant and product ions for detection. The ions are mass analyzed with a double focusing electric/magnetic sector mass filter, and counted with an on-axis conversion/scintillation detector [56]. For these experiments, the ^{52}Cr, ^{55}Mn, ^{56}Fe, ^{96}Mo, and ^{184}W isotopes were selected. The C_{60} sample used in these experiments is from Hoechst and it is 99.9% pure. The oven is heated to ~600 K, and the C_{60} pressure is estimated to be $\sim 10^{-7}$ Torr. This is consistent with the vapor pressure estimated from Knudsen cell data [57] (1.45×10^{-7} Torr). In these experiments, the collision energy is determined by retarding potential analysis of the reactant beam at the point of injection into the scattering octapole. In order to separate the effects of beam energy spread from possible space charge effects on the injection process, retarding potential analyses were run both under normal operating conditions and with beams where the current was attenuated by a factor of ~100 by defocusing at the first mass filter acceleration stage. These low current beams should have the same energy spread, but have less effect from space charge. In fact, little difference was found in retarding behavior, indicating that space charge is not a significant problem under our normal conditions. The zero of the collision energy scale is defined relative to the energy where half the beam is transmitted. This behavior is somewhat different from what we observed in earlier work with rare gas and alkali beams, probably due to the higher currents possible in those systems. The uncertainty in the collision energy scale is roughly 2 eV because of the width of the primary ion beam.

The main problem with our experimental arrangement is that the kinematics for collection of some product ions are poor. The worst case is charge transfer (CT), which we have found [33–35] to give a substantial fraction of slow C_{60}^+, even at high collision energies. For the more interesting dissociative charge transfer (fragmentation) channels, the momentum

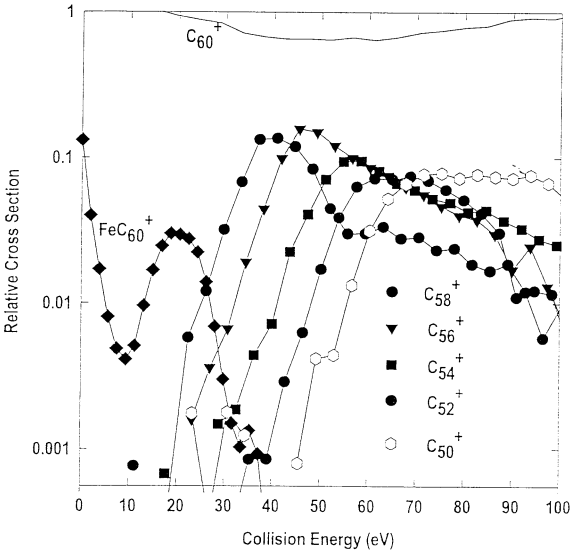

Fig. 1. Collision energy dependence for all significant product channels observed in the reaction of Fe^+ with C_{60}.

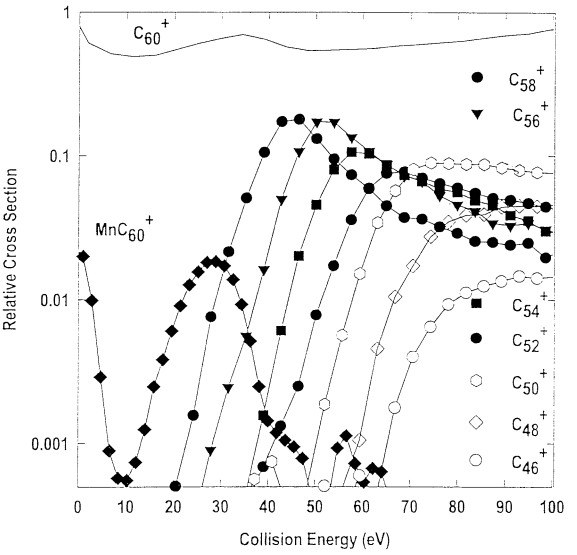

Fig. 2. Collision energy dependence for all significant product channels observed in the reaction of Mn^+ with C_{60}.

transfer approaches 100% inelasticity [35], and thus the product ions are forward scattered with enough energy to be easily collected and detected. The same is true for the MC_{60}^+ complex ions, with the exception that at low collision energies, the products may be slow and difficult to collect. In the plots below we give only relative cross sections. We believe that the uncertainty is quite small (±10%) for the fragment and complex channels, but may be 50% for the C_{60}^+ product.

Compared to the alternative approach [58–65] of scattering fullerene ion beams from atomic or molecular targets, we have two major advantages. Our C_{60} reactant is thermal at 600 K, giving a well defined and relatively cold internal energy distribution compared to typical C_{60}^+ sources. In addition, we are easily able to study reactions with reactive species such as metal ions, where preparation of the corresponding neutral target vapor would be difficult.

3. Results and discussion

The relative cross sections for all observed MC_n^+ and C_n^+ products are plotted in Figs. 1–5 for reaction of Fe^+, Mn^+, Cr^+, Mo^+, and W^+, respectively. Preliminary results for Fe^+, Mn^+, and Mn_2^+ have been reported [28,29], but are replotted for comparison using our current understanding of the correct collision energy scale. Because of uncertainties in collection efficiency and C_{60} target density, each data set has been normalized so that the total cross section at high collision energies is 1.0.

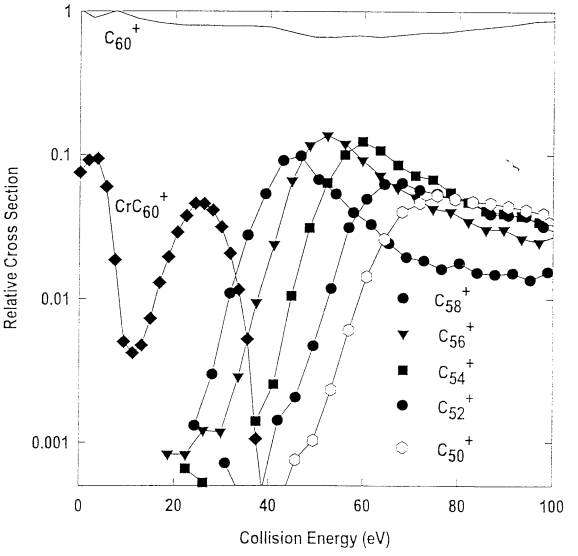

Fig. 3. Collision energy dependence for all significant product channels observed in the reaction of Cr^+ with C_{60}.

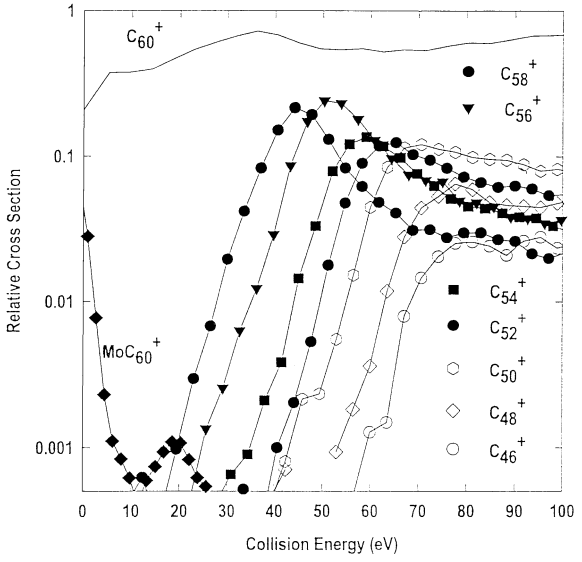

Fig. 4. Collision energy dependence for all significant product channels observed in the reaction of Mo^+ with C_{60}.

3.1. Charge transfer: C_{60}^+

The dominant product channel at all collision energies is charge transfer (CT), [see Eq. (1)] producing C_{60}^+

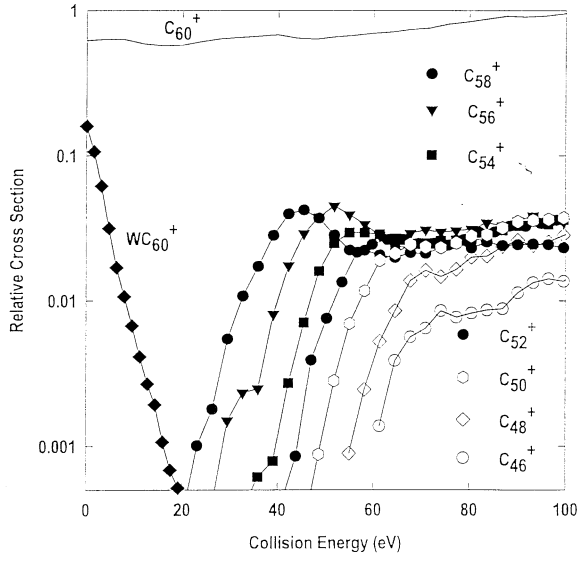

Fig. 5. Collision energy dependence for all significant product channels observed in the reaction of W^+ with C_{60}.

$$M^+ + C_{60} \rightarrow M + C_{60}^+ \quad (1)$$

The only exception is for Mn_2^+, where MnC_{60}^+ dominates at low collision energy. For the metals studied here, the CT energetics vary from 0.26 eV exoergic (Fe^+) to 0.84 eV endoergic (Cr^+), calculated using 7.61 eV for the ionization energy of C_{60} [66], and data for the metals from Lias et al. [67]. Despite the variation in energetics, CT is at least reasonably efficient (our best estimate is that $\sigma > 50$ Å^2) for all five metals, with little dependence on collision energy. Lack of collision energy dependence is consistent with earlier observations [34,35] that C_{60}^+ produced by exoergic CT is very slow in the laboratory frame, i.e. there is little conversion of collision energy in the CT process. Similarly, in alkali ion scattering from C_{60} [36,37], very little endoergic CT is observed, even at collision energies far in excess of the endoergicity. The conclusion is that CT is driven largely by internal energy in the C_{60} product. In our case the 600 K C_{60} have, on average, ~2.5 eV of internal energy. This is large compared to the reactant product energy differences for the transition metal systems, but comparable to the CT endoergicity for the alkalis (2.2 to 3.3 eV for Li to K).

CT continues to dominate the product distribution at high collision energies. This implies that most collisions lead to CT with low enough collision-to-internal energy transfer such that the resulting C_{60}^+ is stable for our 100–800 μs detection time scale. This is consistent with our observation that most CT products have low laboratory velocities [34,35], again indicating little translational inelasticity. We have observed the same behavior for a wide range of atom and molecular ions scattering from C_{60}, and the dynamics are discussed in a recent article [35]. We interpret this behavior as implying that CT occurs mostly in large impact parameter, grazing collisions.

3.2. Fragmentation: C_{60-2n}^+

At high collision energies we observe a series of C_{60-n}^+ fragment ions. A qualitatively similar pattern of successively smaller fragments is observed in all the ion C_{60} scattering studies we have made. For ions

like the rare gases, the fragments are clearly generated by dissociative charge transfer (DCT) events where enough collision energy is converted to internal energy of the nascent C_{60}^+ product to result in decomposition (reaction 2):

$$M^+ + C_{60} \rightarrow M + C_{60}^{+\bullet} \rightarrow C_{58}^+ + C_2 \quad \searrow C_{56}^+ + 2C_2 \quad \searrow \ldots C_{60-2n}^+ + n\,C_2 \qquad (2)$$

For the rare gases, the energetics are reasonably clear, and the principal factors determining the appearance energy of a given fragment are the collision-to-internal energy transfer dynamics and the unimolecular decomposition rate, $k(E)$. Collisional energy transfer determines the amount of internal energy available to drive fragmentation of the nascent C_{60}^+, and the unimolecular decomposition rate determines the extent to which the C_{60}^+ will fragment during the experimental time window. The energy transfer dynamics for rare gas ions are discussed in a recent article dealing with rare gas-C_{60} collision dynamics [35], and we have previously described energy transfer in alkali ion C_{60} collisions [37]. The conclusion reached is that the collisional inelasticity (fraction of collision energy converted to internal energy) approaches unity for a significant fraction of the collisions leading to DCT. Our interpretation is that for nonreactive projectiles, DCT happens primarily in low impact parameter collisions, and at high energies these collisions are highly inelastic. High inelasticity is predicted by any impulsive model [34,37] that takes into account the fact that the collision energy is much higher than the bond energies, so that the projectile interacts with only a few atoms at a time.

From comparison with the rare gas DCT behavior, it is clear that the DCT mechanism (2) cannot account for the fragmentation signal observed at low collision energies for the transition metal cations (TM^+). For example, in $Ar^+ + C_{60}$, the CT process is 8.15 eV exoergic, and most of this electronic energy ends up as internal energy of the nascent C_{60}^+ product. The appearance energy for $Ar^+ + C_{60} \rightarrow C_{58}^+$ is 31 eV. This is consistent with the unimolecular decomposition kinetics reported for C_{60}^+ by Foltin et al. [42], that indicate ~40 eV of internal energy is required in the nascent C_{60}^+ CT product to drive decomposition to $C_{58}^+ + C_2$ within our experimental time window. For the $TM^+ + C_{60}$ systems reported here, where CT is roughly thermoneutral, the DCT mechanism should lead to a C_{58}^+ appearance energy >37 eV (collision energy + thermal energy = 40 eV), while the actual appearance energies are only ~20 eV. In this low collision energy range, at least, the C_{58}^+ must be generated by a chemical reaction:

$$M^+ + C_{60} \rightarrow MC_{60}^{+*} \rightarrow MC_2 + C_{58}^+ \qquad (3)$$

Chemical reactions must also contribute to formation of other C_{60-2n}^+ fragments at higher collision energies, since they uniformly have appearance energies well below those expected for a true DCT process. Most likely, MC_2 elimination (3) allows production of C_{58}^+ with higher internal energies than would be possible for C_2 elimination, and this shifts the appearance energies for daughter fragments as well. Presumably, as collision energy increases, formation of chemically bound MC_{60}^+ becomes less likely, and true DCT processes become more important in the fragmentation channels.

3.3. Low energy adduct

For all the systems studied, an MC_{60}^+ adduct is observed at low collision energies. These adducts have cross sections that decrease rapidly from peak values at low collision energy. For most of the reactants, there is a clear second component that turns on at energies above 10 eV. This high energy component will be discussed in the next section. To allow comparison, the MC_{60}^+ channels for all five transition metal cations are plotted together in Fig. 6.

In our single collision environment, adducts are unstable with respect to dissociation, either back to reactants or to products. The collision energy dependence is determined by two factors. If there were an activation barrier for formation of the MC_{60}^+, we would see threshold behavior. With one exception, all

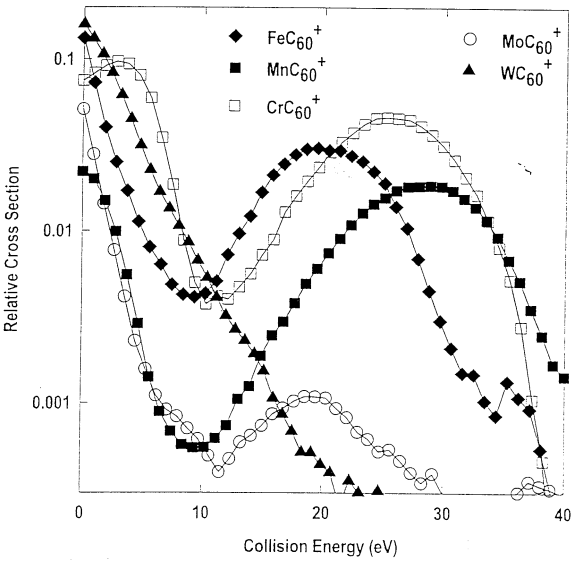

Fig. 6. Comparison of the cross sections of the MC_{60}^+ adducts.

the MC_{60}^+ cross sections peak at low energies, indicating that any barriers to MC_{60}^+ formation are too small to significantly affect the formation probability at low collision energy, bearing in mind that our 600 K C_{60} reactant has an average internal energy of 2.5 eV. For CrC_{60}^+, the cross section does turn over at low energies, possibly due to a barrier. Note, however, that adduct collection efficiency at low collision energies is problematic and the turnover could be an artifact. Once formed, the probability that MC_{60}^+ survives to be detected depends on the unimolecular decomposition time constant and the flight time to the detector. The flight time is well defined since it is just determined by the velocity of the center-of-mass in the lab frame, and is a few milliseconds for these low energy collisions. As the collision energy increases, the energy available to drive unimolecular decomposition increases, and the decomposition rate increases roughly exponentially. Since the flight time decreases only slowly with increasing collision energy, the survival probability rapidly decreases.

In the collision energy range where the low energy adduct disappears, the only significant product species is C_{60}^+. This implies that the only possible decomposition channels are:

$$MC_{60}^{+*} \rightarrow M^+ + C_{60} \quad \text{and} \quad MC_{60}^{+*} \rightarrow M + C_{60}^+ \tag{4}$$

Neither channel can be monitored directly because of interference from the primary M^+ beam and from the C_{60}^+ charge transfer product. Given that CT occurs with similar cross sections for all transition metal ions studied, independent of the exo/endoergicity of the CT reaction, it seems likely that both MC_{60}^+ decomposition channels are important.

We can fit the collision energy dependence of the low energy adduct signal with an RRKM-based simulation of the experiment [35], and extract an estimate of the $(M - C_{60})^+$ binding energy. These turn out to be in the 1–3 eV range, but we are not able to give more precise values because of the sensitivity of the extracted binding energy to the collision energy uncertainty.

Our observations of a low energy adduct are consistent with earlier experiments by Freiser and co-workers [25] who observed formation of a FeC_{60}^+ complex from the reaction of $[FeC_nH_{2n}]^+$ (n = 2–5) with C_{60} at thermal energies. Based on their results, they proposed that this low energy species is an exohedral coordination complex. That structure is consistent with the observation that there is little or no activation barrier to MC_{60}^+ formation. Freiser and co-workers estimated that the $Fe - C_{60}^+$ binding energy is ~1.7 eV, again consistent with our estimate. In another experiment, Freiser and co-workers [68] reported that collision-induced dissociation of MC_{60}^+ yields $C_{60}^+ + M$, when M = Fe, Ni, Co, and Cu, and yields C_{60} and M^+ when M = La and VO. RhC_{60}^+ yields a mixture of C_{60}^+ and Rh^+. The branching between the two product charge states depends on the relative ionization energies of C_{60} and the metal atom. Because of interference from the primary beam and from CT products, we are not able to address the branching.

Welling et al. [69] generated and stored a MgC_{60}^+ complex inside a linear ion trap. The MgC_{60}^+ adduct was prepared by reacting Mg^+ ions generated externally by electron impact with neutral C_{60} vapor molecules. The dissociation of this adduct in the ion trap was followed by mass spectrometry and laser

induced fluorescence. They found two competing dissociation channels for single photon excited MgC_{60}^+ [Eq. 5 (a) and (b)]

$$MgC_{60}^+ \rightarrow C_{60}^+ + Mg \quad (5a)$$

$$MgC_{60}^+ \rightarrow C_{60} + Mg^+ \quad (5b)$$

with the first channel [Eq. (5a)] dominating, in agreement with the ionization energies of Mg and C_{60} (IE for Mg = 7.644 eV, slightly more than IE of C_{60} = 7.61). They attributed the second decay channel to the photoexcited MgC_{60}^+ complexes. They suggest an exohedral complex of MgC_{60}^+ adduct.

The relatively weak binding of these exohedral complexes is consistent with them being coordination compounds. The metal atom could conceivably be coordinated to a single carbon atom (η^1), to a pair of carbon atoms at either a pentagon–hexagon or hexagon–hexagon boundary (both η^2), or to the π cloud of a pentagon (η^5) or hexagon (η^6) [70]. Bohme and co-workers [27] prepared FeC_{60}^+ by ion molecule reaction in a selected ion flow tube. Reaction of the FeC_{60}^+ with N_2O and CO was studied, and they concluded that FeC_{60}^+ was dihapto coordinated to a 6–6 double bond of the fullerene.

It has also been shown by x-ray diffraction that transition metals bind to C_{60} in a dihapto fashion, where carbon–carbon double bonds of C_{60} act like those of alkenes rather than aromatic molecules such as benzene [23]. It has been shown theoretically that η^2 coordination above two carbon atoms between two hexagons is favored [70] over other sites. The preference of η^2 bonding over η^5 or η^6 [68] is due to the fact that the *p*-orbitals of the pentagonal or hexagonal rings of the fullerene molecule are tilted away from the center of the ring because of the curvature of the C_{60} cage.

In these exohedral complexes the transition metal atom coordinated to C_{60} has a clear effect on the C_{60} cage. In $[(C_6H_5)_3P]_2Pt(\eta^2 - C_{60}) \times (C_4H_8O)$ it has been shown that the two carbon atoms coordinated to the Pt are displaced outward from their positions in C_{60}. Using EXAFS Pradeep and co-workers [16] found that Fe–C distances for FeC_{60} prepared from a solution reaction are 2.03 and 3.46 Å. They suggested that the metal-C_{60} bond in this adduct is the weakest, consistent with the observation by us and others, that MC_{60}^+ dissociates by metal loss.

In summary, we believe that the adduct observed at low collision energies is an exohedral coordination complex, bound by 1–3 eV, consistent with observations in other groups that such complexes form in thermal energy collisions. Even though the binding energies for these exohedral complexes are 1–3 eV, they survive to ~10 eV (~12.5 eV average internal energy) because of the large number of degrees of freedom available to store the excess energy.

3.4. Nature of the "high energy" adduct

The most interesting feature of our results is the second, higher energy component of the cross section for MC_{60}^+ formation. The collision energy dependence of this adduct shows that it is chemically distinct from the exohedral adduct formed at low collision energies. For Fe^+, Mn^+, Cr^+, and Mo^+, the high energy component is clearly separated from the exohedral (low energy) adduct by a sharp minimum where intensity drops by at least an order of magnitude. Visual inspection of the cross sections indicates that the appearance energies for the four high energy adducts are all in the 8–10 eV range. The implication is that formation of this adduct requires a substantial activation collision energy, and this activation energy is roughly the same for the four cations.

For W^+, there is only a single cross section component, however, this component extends to collision energies well beyond the point where the low energy components for the other reactant ions have disappeared. One possible explanation would be that the WC_{60}^+ exohedral coordination complex has a substantially larger binding energy than for the other transition metals studied, and that the high energy adduct observed for the other metals does not form for W^+. As Fig. 6 shows, however, the trends observed for the other metals suggests a different interpretation. Note that when we go down the periodic table from Cr^+ to Mo^+, the collision energy range where the high energy adduct is observed shifts to lower energies, indicating that the high energy adduct becomes

less stable. If this trend continues, we would expect that the WC_{60}^+ high energy adduct would appear at even lower collision energies, possibly merging into the low energy component. Note that there is also a hint of a shoulder in the WC_{60}^+ signal at collision energies above ~10 eV. Taken together, these observations suggest that the single broad component observed for WC_{60}^+ is actually composed of overlapping low and high energy components.

The observation that the high energy adduct survives to be detected (200–300 μs) for collision energies of 30–40 eV, implies that its binding energy is substantially higher than the 1–3 eV binding of the exohedral coordination adduct observed at low energies. In contrast to the rather similar 8–10 eV appearance energies, the peak energies and disappearance energies are quite different for the different transition metals. The MnC_{60}^+ cross section peaks near 30 eV, and falls to 10% of its peak value near 40 eV. In contrast, the MoC_{60}^+ cross section peaks near 20 eV, and the adduct has essentially vanished by 30 eV. If our deduction that the WC_{60}^+ high energy component is merged with its low energy component is correct, the implication is that WC_{60}^+ only survives to ~25 eV.

The appearance energy of the high energy adducts is a measure of the collision energy required to drive the system over the activation barrier to adduct formation. The energy where the MC_{60}^+ signal peaks is determined by the energy dependence of both the formation cross section and the survival probability, and therefore is not easily related to energetics. Note that all the adduct cross sections have a relatively sharp high energy limit (cut-off energy). This sharp drop is expected for unimolecular decay of MC_{60}^+ because the internal energy increases linearly with collision energy [$E_{\text{int}} = E_{\text{col}} + E_{\text{thermal}}(C_{60})$], and the unimolecular lifetime decreases approximately exponentially with excess energy. As the internal energy is increased, the lifetime of the adducts eventually drops below the experimental observation time, and adducts are no longer detected. The observation time is determined by the flight time from the scattering cell to the mass spectrometer, varies with both collision energy and ion mass, and can easily be included in modeling of the data.

The large variation in cut-off energies for MC_{60}^+ implies a significant variation in the stability of the MC_{60}^+ adducts. Note that in the Cr–Mo–W series, the mass of the projectile increases, and this results in faster MC_{60}^+, and therefore, shorter detection flight times. If these three adducts had similar stability we would expect the cut-off energies to increase from Cr to W, however, the opposite is observed. Quantitative modeling is discussed below.

A major question is the structure of the high energy adduct. We have seen that there is a significant activation barrier to forming the adduct and that the barrier is not strongly dependent on metal. The large barrier argues for an adduct formation process requiring C–C bond breaking. The adduct is also chemically bound, with bond energies in the 3–6 eV range (see below). Since exohedral coordination seems to give rise to an activationless, weakly bound adduct, a different bonding scheme is required.

One clue as to the structure is the approximately metal-independent 8–10 eV appearance energy. Another clue is the decomposition product distribution for the adduct. The low energy exohedral adduct decays entirely by M or M^+ elimination, as shown above. Based on the other ions observed in the collision energy range where the high energy adduct decomposes, two product pairs are possible:

$$MC_{60}^+ \rightarrow M^+ + C_{60} \quad \text{or} \quad M + C_{60}^+$$
$$\rightarrow MC_2 + C_{58}^+ \quad \text{or} \quad MC_2^+ + C_{58} \qquad (6)$$

M^+ and C_{60}^+ products are obscured by the primary ion beam and charge transfer products, respectively, and cannot be ruled out. C_{58}^+ also suffers interference from dissociative charge transfer (DCT), however as explained above, the DCT process cannot explain the C_{58}^+ signal observed for collision energies below ~37 eV. Comparison of the intensities of the MC_{60}^+ and C_{58}^+ signals indicates that MC_2 loss is a major decomposition channel for the high energy adduct. Indeed, for the more weakly bound Mo^+ and W^+ adducts, only a small fraction of the adduct survives to be detected, and the major signature of the $M^+ + C_{60} \rightarrow MC_{60}^+ \rightarrow MC_2 + C_{58}^+$ process is the appearance of C_{58}^+ at low energies. As a further check on the importance

of the $(MC_2 + C_{58})^+$ decomposition product pair, we looked for MC_2^+ production. Because of the very different product collection/detection kinematics for the light fragment ion, it is not possible to generate a quantitative estimate of the relative branching to $MC_2 + C_{58}^+$ versus $MC_2^+ + C_{58}$, however, MC_2^+ is produced in the collision energy range where MC_{60}^+ is decomposing.

There are two obvious binding arrangements for the high energy adduct. For rare gases and alkalis, we have found that endohedral adducts, where the heteroatom is physically trapped inside the cage, are important [35,37]. Indeed, in our preliminary reports on Fe^+ and Mn^+ scattering from C_{60} [28, 29] we speculated that an endohedral complex might be responsible for the high energy adduct in these systems. In this scenario, the activation barrier results from the kinetic energy required to displace carbon atoms to open a hole for the projectile atom to enter. In the rare gas and alkali systems, we studied the penetration threshold behavior as a function of projectile size and mass, and found that the threshold energy increases substantially with size. The penetration threshold increases from 30–43 eV from Ar^+ to Xe^+, and the results for the alkalis are similar.

There are several aspects of the observations that are difficult, but not impossible, to reconcile with typical endohedral complex behavior. For atoms the size of the transition metal monocations, we would expect AEs for the high energy adduct in the 30–40 eV range—far higher than the 8–10 eV observed. This might be rationalized by assuming that penetration is assisted by chemical interactions, i.e. metal carbon interactions that weaken the fullerene cage around the impact site [16,23]. In addition, the rare gas and alkali endohedrals we have studied all decompose primarily by C_2 elimination, leading to a series of $A@C_{60-2n}^+$ endohedral fragment ions. In contrast, the MC_{60}^+ adducts decompose entirely by elimination of MC_2/MC_2^+ and possibly M^+/M, and the binding energy (see below) is metal dependent. A difference in decomposition energetics is not unexpected. The rare gas atoms and alkali cations involved in those endocomplexes are closed shell and do not interact strongly with the cage walls. The transition metal atoms/cations, on the other hand, are able to form chemical bonds that might weaken the bonding in the carbon atoms around the attachment site. Just as weakened CC bonding might explain the lowered penetration thresholds, it may also account for the preference for MC_2/MC_2^+ elimination, and the reduced stability relative to C_{60}^+ itself [42].

Decomposition has been studied for a few endohedral metallo-fullerenes, and these results also tend to argue against an endohedral structure for our adducts. For example, Pradeep et al. [16] observed peaks in mass spectra due to C_2 and C_4 losses from FeC_{60}^+ generated from arc vaporization of graphite in an atmosphere of $Fe(CO)_5$, while our FeC_{60}^+ always loses the metal atom when decomposing. Lorents et al. [71] found that fragmentation of endohedral $M@C_{82}^+$, M = La and Gd, by energetic collision with various atomic and molecular targets, went by loss of C_2 units, producing $M@C_{2n}^+$ ($30 \leq n \leq 40$) and by loss of metal-containing fragment ions MC_{2n}^+ ($0 \leq n \leq 5$). On the other hand, Achiba et al. [72] and Lorents et al. [71] have observed metal dicarbide elimination from endohedral metallo-fullerenes upon laser or collisional excitation. Taking all this together, we believe that our high energy adducts are most likely not endohedral complexes, but we cannot rule out this possibility.

We feel that the more likely structure for the high energy adduct has the metal bound into the C_{60} network, inserted into one or more CC bonds. For geometric reasons, the metal atom cannot simply embed in the surface of the C_{60}, and must either protrude inside or outside the sphere of carbon atoms (exohedral network bonding). Based on the 8–10 eV AEs adduct formation, relative to the 30–40 eV expected penetration energy, we feel that the metal atoms mostly remain external to the cage. Note that Jarrold and co-workers [32] have shown that transition metals can form exohedral network isomers with fullerenes. At higher energies (>40 eV), it is not unlikely that the metal sometimes ends up bound to the inside surface of the sphere, corresponding to a type of endohedral complex.

For the exohedral network structure, the observed metal-independent 8–10 eV collision energy thresh-

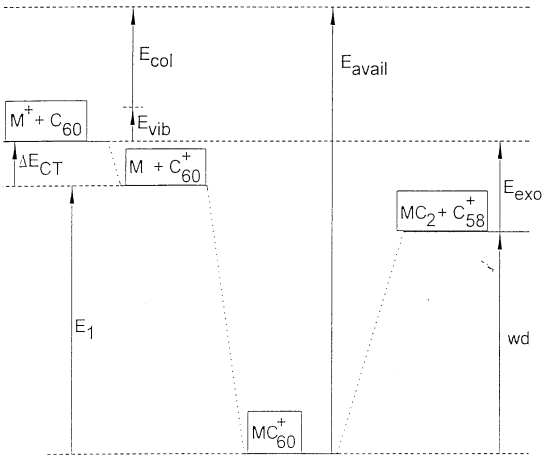

Fig. 7. Energetic diagram for the interaction of transition metal ions with C_{60}.

old can be rationalized as the kinetic energy required to break CC bonds and distort the carbon cage to allow insertion of the metal atom into the carbon network. Our results do not provide much insight into details of the bonding, however, insertion into a single CC bond is perhaps most consistent with intuition and with the observation that metal dicarbide elimination is the dominant decomposition pathway.

4. Dissociation energy of MC_{60}^+

We would like to extract from our data an estimate of the adduct binding energy. A schematic energy diagram for reaction of M^+ with C_{60} is shown in Fig. 7, for the case where CT is exoergic. In cases where CT is endoergic, a similar diagram can be drawn. E_{col} is the collision energy, E_{vib} is the thermal vibrational energy in the 600 K C_{60} target molecules ($\langle E_{vib} \rangle \approx$ 2.5 eV), ΔE_{CT} is the charge transfer exoergicity, E_1 is the binding energy of the adduct with respect to $M + C_{60}^+$, wd is the well depth with respect to $MC_2 + C_{58}^+$ products, E_{exo} is the net exoergicity of the reaction forming C_{58}^+, and E_{avail} is the total energy available to drive the reaction. E_{avail} is equal to the sum of E_{col}, E_{vib}, E_{CT}, and E_1. Because the energetics for these systems are not well established, we have two unknown energetic parameters, wd and E_{exo}. Some thermochemical information is available on metal dicarbides, [67], and many different values are available for the dissociation energy of C_{60}^+ into $C_{58}^+ + C_2$. Putting this information together we estimate that E_{exo} is likely to be in the range between ± 2 eV.

In simpler cases such as decomposition of C_{60}^+ or of rare gas endohedrals, only one energetic parameter is unknown, and the experimental decomposition versus energy behavior can be fit to extract the desired energetics. For example, Foltin et al. [42] have reported a careful RRKM/QET based analysis of C_{60}^+ breakdown that has yielded a widely used number for the dissociation energy of C_{60}^+ to $C_{58}^+ + C_2$. Even in these simpler systems there is considerable disagreement regarding the best fitting process, the importance of radiative effects, and the value of the resulting dissociation energy. A major source of uncertainty is the nature of the transition state governing the dissociation process. For example, from our rare gas endohedral data [34,35], we can extract the decomposition (C_2 elimination) rate as a function of E_{avail}, and can fit the results using an RRKM-based simulation of our experiment. If we use a transition state similar to that used by Foltin et al. [42], we get a dissociation energy very close to the 7.1 eV value they extract for C_{60}^+. As expected, the presence of an endohedral rare gas atom has little effect on the cage properties. If, on the other hand, we vary the transition state properties from rather tight to near orbiting, it is possible to extract dissociation energies that vary by $\pm 50\%$. Fundamentally, the problem is that the decomposition rates for such large molecules increase so slowly with excess energy that experimental data would be required over an impossibly large dynamic range in order to unambiguously determine the dissociation energy.

In the MC_{60}^+ adducts observed here, there is the additional complication that two energetic parameters are unknown, thus the RRKM model is underdetermined. We have found, however, that it is possible to get a good estimate of the adduct binding energy (wd) from our data. This is done by running a series of RRKM-based simulations of the adduct breakdown energy dependence, varying E_{exo} within a chemically reasonable range (± 2 eV). It turns out that within this

Table 1
Some physical properties of transition metal ions

Metal ions	IE (eV)	Ionic size (Å)	ΔH (CT)
Fe	7.87	0.8	−0.26
Mn	7.435	0.8	0.17
Cr	6.766	0.73	0.84
Mo	7.099	0.70	0.51
W	7.6	0.65	0.0

range of E_{exo}, the extracted wd parameters vary by only ~0.3 eV. Since this is far smaller than the uncertainty in wd from not knowing the properties of the transition state, we feel that the binding energy numbers are at least useful as semiquantitative estimates. The approach used in the breakdown modeling is essentially identical to that used for the rare gas endohedral complexes, and details can be found in earlier papers. For these simulations, we used a transition state model similar to that of Foltin et al. [42], and our results are, therefore, dependent on the unknown accuracy of this assumption. Our rationale for using this model is that it, and the resulting 7.1 eV C_{60}^+ dissociation energy, are well known and provide a point of comparison for MC_{60}^+.

The most strongly bound adduct MnC_{60}^+, with $D(MnC_2 - C_{58}^+)$ estimated to be 5.8 eV. This is substantially lower than the 7.1 eV value for $D(C_2 - C_{58}^+)$, supporting the idea that the metal-carbon bond formation weakens the neighboring CC bonds. For iron and chromium the simulations gave nearly identical dissociation energies of 5.2 eV. For the heavier transition metals the dissociation energy decreases: $D(MoC_2 - C_{58})^+ = 4.3$ eV and $D(WC_2 - C_{58})^+ = 3.5$ eV. This decrease in MC_2-loss energy probably reflects greater disruption of the C–C bonding for the heavier transition metals. As noted, there is insufficient information about MC_2 molecules to more closely analyze the periodic trend.

5. Summary

We have demonstrated that the five transition metal cations studied all form both a weakly bound exohedral coordination complex, and a more strongly bound complex that we tentatively attribute to insertion of the metal atom into a C–C bond (network binding). The network adduct decomposes largely by MC_2/MC_2^+ elimination, and estimates are given for the energetics.

Acknowledgements

Construction of the instrument used in this work was supported by the Office of Naval Research (Mechanics and Energy Conversion Division N0001492J1202). Partial support was from a Camille and Henry Dreyfus Foundation Teacher-Scholar Award to S.L.A. We are also grateful to Professor P.B. Armentrout for fruitful discussions regarding metal cation chemistry.

References

[1] Y. Chai, T. Guo, C. Jin, R.E. Haufler, L.P.F. Chibante, J. Fure, L. Wang, J. Michael Alford, R.E. Smalley, J. Phys. Chem. 95 (1991) 7564.
[2] H. Shinohara, H. Sato, Y. Saito, M. Ohkohchi, Y. Ando, J. Chem. Phys. 96 (1992) 3571.
[3] E. Yamamoto, M. Tansbo, T. Tomiyama, H. Shinohara, Y. Kobayashi, J. Am. Chem. Soc. 118 (1996) 2293.
[4] Y. Saito, S. Yokoyama, M. Inakuma, H. Shinohara, Chem. Phys. Lett. 250 (1996) 80.
[5] Z. Xu, T. Nakane, H. Shinohara, J. Am. Chem. Soc. 118 (1996) 11309.
[6] R.D. Johnson, M.S. de Vries, J. Salem, D.S. Bethune, C.S. Yannoni, Nature 355 (1992) 239.
[7] D.S. Bethune, C.H. Kiang, M.S. de Vries, G. Gorman, R. Savoy, H.A. Jimenez-Vazquez, R. Beyers, Nature 363 (1993) 605.
[8] M.M. Ross, H.H. Nelson, J.H. Callahan, S.W. McElvany, J. Phys. Chem. 96 (1992) 5231.
[9] E.G. Gillan, C. Yeretzian, K.S. Min, M.M. Alvarez, R.L. Whetten, R.B. Kaner, J. Phys. Chem. 96 (1992) 6869.
[10] S. Suzuki, S. Kawata, H. Shiromaru, K. Yamauchi, K. Kikuchi, T. Kato, Y. Achiba, J. Phys. Chem. 96 (1992) 7159.
[11] K. Kikuchi, S. Suzuki, Y. Nakao, N. Nakahara, T. Wakabayashi, H. Shiromaru, I. Saito, I. Ikemoto, Y. Achiba, Chem. Phys. Lett. 216 (1993) 67.
[12] W. Sliwa, Transition Met. Chem. 21 (1996) 583.
[13] M. Takada, B. Umeda, E. Nishibori, M. Sakata, Y. Saito, M. Ohno, H. Shinohara, Nature 377 (1995) 46.
[14] K. Kikuchi, Y. Nakao, S. Suzuki, Y. Achiba, T. Suzuki, T. Maruyama, J. Am. Chem. Soc. 116 (1994) 9367.

[15] H. Shinohara, M. Inakuma, N. Hayashi, H. Saito, T. Kato, T. Bandow, J. Phys. Chem. 48 (1994) 8597.
[16] T. Pradeep, J. Am. Chem. Soc. 114 (1992) 2272.
[17] R. Beyers, C.H. Kiang, R.D. Johnson, J.R. Salem, M.S. de Vries, C.S. Yannoni, D.S. Bethune, H.C. Dorn, K. Harich, S. Stevenson, Nature 370 (1994) 196.
[18] L. Soderholm, P. Wurz, K.R. Lykke, D.H. Parker, F.W. Lytle, J. Phys. Chem. 96 (1992) 7153.
[19] Y. Kubozono, T. Urakawa, Y. Yoshida, H. Maeda, H. Ishida, Y. Furukawa, K. Yamada, S. Kashino, Chem. Phys. Lett. 225 (1996) 19.
[20] D.W. Cagle, T.P. Thrash, M. Alford, L.P. Felipe Chibante, G.J. Ehrhardt, L. Wilson, J. Am. Chem. Soc. 118 (1996) 8043.
[21] J. Laskin, H.A. Jimenez-Vasquez, R. Shimshi, M. Saunders, M.S. de Vries, C. Lifshitz, Chem. Phys. Lett. 242 (1995) 249.
[22] R.E. Douthwaite, M.L.H. Green, A.H.H. Stephens, J.F.C. Turner, J. Chem. Soc., Chem. Commun. (1993) 1522.
[23] P. Fagan, J. Calabrese, B. Malone, Acc. Chem. Res. 25 (1992) 134.
[24] A. Hirsch, Synthesis (1995) 895.
[25] L.M. Roth, Y. Huang, J.T. Schwedler, C.J. Cassady, D. Ben-Amotz, B. Kahr, B.S. Freiser, J. Am. Chem. Soc. 113 (1991) 6298.
[26] S.W. McElvany, J. Phys. Chem. 96 (1992) 4935.
[27] V. Baranov, D. Bohme, Int. J. Mass Spectrom. Ion Processes 149/150 (1995) 543.
[28] Y.J. Basir, Z. Wan, J.F. Christian, S.L. Anderson, Int. J. Mass Spectrom. Ion Processes 138 (1994) 173.
[29] Y.J. Basir, S.L. Anderson, Chem. Phys. Lett. 243 (1995) 45.
[30] J.F. Christian, Z. Wan, S.L. Anderson, J. Phys. Chem. 96 (1992) 10597.
[31] K. Shelimov, M.F. Jarrold, J. Am. Chem. Soc. 117 (1995) 6404.
[32] K. Shelimov, D.E. Clemmer, M.F. Jarrold, J. Chem. Soc. Dalton Trans. (1996) 567.
[33] Z. Wan, J.F. Christian, S.L. Anderson, J. Chem. Phys. 96 (1992) 3344.
[34] J.F. Christian, Z. Wan, S.L. Anderson, J. Chem. Phys. 99 (1993) 3468.
[35] Y. Basir, S.L. Anderson, J. Chem. Phys. 107 (1997) 8370.
[36] Z. Wan, J.F. Christian, S.L. Anderson, Phys. Rev. Lett. 69 (1992) 1352.
[37] Z. Wan, J.F. Christian, Y. Basir, S.L. Anderson, J. Chem. Phys. 99 (1993) 5858.
[38] J.F. Christian, Z. Wan, S.L. Anderson, Chem. Phys. Lett. 199 (1992) 373.
[39] J.F. Christian, Z. Wan, S.L. Anderson, J. Phys. Chem. 96 (1992) 3574.
[40] P. Wurz, R.N. Lykke, J. Phys. Chem. 96 (1992) 10 129.
[41] C. Lifshitz, P. Sandler, H. Schwarz, H.F. Grutzmacher, J. Sun, T. Weiske, J. Phys. Chem. 97 (1993) 6592.
[42] M. Foltin, M. Lezius, P. Scheier, T.D. Märk, J. Chem. Phys. 98 (1993) 9624.
[43] S.C. O'Brien, J.R. Heath, R.F. Curl, R.E. Smalley, J. Chem. Phys. 88 (1988) 220.
[44] J.U. Andersen, C. Brink, P. Hvelplund, M.O. Larsson, B. Beck Nielsen, H. Shen, Phys. Rev. Lett. 77 (1996) 3991.
[45] E. Kolodney, A. Budrevich, B. Tsipingyuk, Phys. Rev. Lett. 74 (1995) 510.
[46] K. Hansen, O. Echt, Phys. Rev. Lett. 78 (1997) 2337.
[47] C. Lifshitz, I. Gotkis, P. Sandler, J. Laskin, Chem. Phys. Lett. 200 (1992) 406.
[48] R. Mitzner, E.E.B. Campbell, J. Chem. Phys. 103 (1995) 2445.
[49] K. Hansen, E.E.B. Campbell, J. Chem. Phys. 104 (1996) 5012.
[50] Y.J. Basir, J.F. Christian, Z. Wan, S.L. Anderson, Int. J. Mass Spectrom. Ion Processes 171 (1997) 159.
[51] J.L. Elkind, P.B. Armentrout, J. Phys. Chem. 90 (1986) 5736.
[52] F. Strobel, D.P. Ridge, J. Phys. Chem. 93 (1989) 3635.
[53] J.L. Elkind, P.B. Armentrout, J. Chem. Phys. 84 (1986) 4862.
[54] W.D. Reents, F. Strobel, R.B. Freas, J. Wronka, D.P. Ridge, J. Phys. Chem. 89 (1985) 5666C.
[55] C.E. Moore, Atomic Energy Levels (Vols. 1–3) (Natl. Stand. Ref. Data Ser. (U.S., Natl. Bur. Stand.) (Washington, DC, 1971).
[56] H.M. Gibbs, E.D. Commins, Rev. Sci. Instrum. 37 (1966) 1385.
[57] C.K. Mathews, M.S. Baba, T.S.L. Narasimhan, R. Balasubramanian, N. Sivaraman, T.G. Srinivasan, P.R.V. Rao, J. Phys. Chem. 96 (1992) 3566.
[58] T. Weiske, D.K. Bohme, J. Hrušák, W. Krätschmer, H. Schwarz, Angew. Chem. 103 (1991) 989.
[59] T. Weiske, D.K. Bohme, J.D. Hrušák, W. Krätschmer, H. Schwarz, Angew. Chem. Int. Ed. Engl. 30 (1991) 884.
[60] T. Weiske, H. Schwarz, D.E. Giblin, M.L. Gross, Chem. Phys. Lett. 227 (1994) 87.
[61] M.M. Ross, J.H. Callahan, J. Phys. Chem. 95 (1991) 5720.
[62] K.A. Caldwell, D.E. Giblin, M.L. Gross, J. Am. Chem. Soc. 114 (1992) 3743.
[63] J. Hrušák, D.K. Bohme, T. Weiske, H. Schwarz, Chem. Phys. Lett. 193 (1992) 97.
[64] R.C. Mowrey, M.M. Ross, J.H. Callahan, J. Phys. Chem. 96 (1992) 4755.
[65] E.E.B. Campbell, R. Ehlich, J.M.A. Frazao, I.V. Hertel, Z. Phys. D 23 (1992) 1.
[66] J.A. Zimmerman, J.R. Eyler, S.B. Bach, S.W. McElvany, J. Chem. Phys. 94 (1991) 3556.
[67] S.G. Lias, J.E. Bartmess, J.F. Liebman, J.L. Holmes, R.D. Levin, J. Phys. Chem. Ref. Data 17 (1988) 1–861 (suppl. 1).
[68] Y. Huang, B.S. Freiser, J. Am. Chem. Soc. 113 (1991) 9418.
[69] M. Welling, R.I. Thompson, H. Walther, Chem. Phys. Lett. 253 (1996) 37.
[70] H.G. Busmann, T. Lill, B. Reif, I.V. Hertel, Surf. Sci. 272 (1992) 146.
[71] D.C. Lorents, D.H. You, C. Brink, N. Jensen, P. Hvelplund, Chem. Phys. Lett. 236 (1995) 141.
[72] M. Ishibashi, Y. Tomioka, Y. Taniguchi, S. Suzuki, T. Wakabayashi, Y. Kojima, K. Kikichi, Y. Achiba, Jpn. J. Appl. Phys. 33 (1994) 1265.